Sensitivity of out-of-plane capacity to input parameters of Nepali URM walls

Nicola Giordano[a], Flavia De Luca[a], Prem Nath Maskey[b], Anastasios Sextos[a]
[a] *Department of Civil Engineering, University of Bristol, Bristol, UK*
[b] *Department of Civil Engineering, Tribhuvan University, Kathmandu, Nepal*

Keywords: Sensitivity analysis, tornado diagram, out-of-plane, masonry, Nepal, schools

ABSTRACT
Out-of-plane (OOP) is a recurrent seismic damage pattern for unreinforced masonry (URM) constructions. It is usually triggered by insufficient wall-to-wall and wall-to-floor connections. This situation is rather common in Nepal where most of the URM buildings lack of seismic detailing. Therefore, to execute a reliable vulnerability assessment, OOP needs to be considered when dealing with Nepalese masonry constructions. This is generally done by calculating the wall OOP capacity in terms of a force-displacement (*F-D*) curve. By adopting an analytical solution previously developed by the authors, this work investigates the sensitivity of out-of-plane failure to uncertain input parameters of Nepali URMs. A representative wall from a typical single-story brick-in-mud school building is considered in the analysis. Tornado diagrams are adopted to quantify the influence of the seven relevant input quantities over the OOP force-displacement curve. The results of the sensitivity analysis can be used to prioritize data collection and material testing for the most influential parameters.

1 INTRODUCTION

It is nowadays well known that out-of-plane (OOP) seismic damage is a recurrent pattern in unreinforced masonry (URM) buildings (e.g., De Felice and Giannini, 2001; Giaretton et al., 2017). Lack of wall-to-wall and wall-to-floor connections, absence of seismic detailing and excessive flexibility of the horizontal structures are generally the main factors that trigger OOP damage (Ferreira et al., 2015a). Therefore, when most of the building stock is constituted by structurally deficient URMs, it is fundamental to include the OOP assessment in fragility and vulnerability analyses (e.g., Ceran and Erberik, 2013; Ahmad et al., 2014).

These considerations certainly apply to the case of Nepal. Due to the poor construction quality, in the aftermath of the 2015 Gorkha earthquake, OOP failures were largely documented (Sharma et al. 2016; Brando et al., 2017). Accounting for OOP damage is then a crucial aspect in the assessment of Nepalese buildings (De Luca et al., 2019).

Many procedures are available in the literature to account for OOP damage potential (e.g., D'Ayala and Paganoni, 2011; Lagomarsino and Cattari, 2015). The spectral-based techniques rely on the estimation of the OOP force-displacement (*F-D*) curve of building walls. *F-D* curves can be calculated with simplified closed/form equations (Doherty et al., 2002; Ferreira et al., 2015b), analytical procedures (La Mendola et al. 1995; Godio and Beyer, 2017) or numerical modelling (De Felice and Giannini, 2001). Recently, a novel analytical closed-form solution for the estimation of *F-D* curves has been developed and adopted to derive OOP fragility curves for brick-in-mud URM schools in Nepal (Giordano et al., 2019).

By adopting this analytical formulation, the present work investigates the sensitivity of OOP capacity to uncertain parameters of Nepali URM walls. Tornado diagrams are adopted for the case. The study is carried out considering an illustrative URM wall of a typical single-story brick-in-mud school in Nepal. The relevance of sensitivity results is finally discussed with respect to prioritization of data collection and material testing.

2 OUT-OF-PLANE ANALYTICAL MODEL

The analytical closed-form solution adopted in this study is based on the following assumptions: (i) the OOP capacity of an URM wall is governed by bending (La Mendola et al. 1995; Shawa et al., 2012); (ii) depending on the boundary conditions (i.e., cantilever, clamped-clamped, pinned-pinned) the wall is discretized as a system of rigid bodies and nonlinear hinges; (iii) the cracking response of masonry at cross-section level is simulated by the nonlinear hinges; (iv) the moment-rotation (*M-θ*)

relationship of the nonlinear hinges depends on the moment-curvature (M-χ) response of the critical cross-section (Giordano et al. 2017); (v) to obtain the M-θ relationship from the M-χ, an integration length L_i is defined. In particular, experimental versus numerical calibration provided L_i = 0.25 h_{LV}, where h_{LV} is the shear length of the wall. Referring to the cantilever configuration, the model consists of one rigid body connected to the ground with one nonlinear hinge. By imposing the rotational equilibrium around the hinge, the OOP F-D curve of the wall is derived:

$$F = \frac{1}{h\alpha_h}\left(\frac{1}{12}E_m B t^3 \frac{D}{L_i h} - \frac{WD}{2} - ND\right) \quad for\ D \le L_i h \frac{2(W+N)}{E_m B t^2} \tag{1}$$

$$F = \frac{1}{h\alpha_h}\left[(N+W)\left(\frac{t}{2} - \sqrt{\frac{2L_i t(N+W)}{9E_m BD}}\right) - \frac{WD}{2} - ND\right] \quad for\ L_i h \frac{2(W+N)}{E_m B t^2} \le D \le L_i h \frac{{f_{mb}}^2 B}{2E_m(W+N)} \tag{2}$$

where: F is the base shear of the wall, D is the top displacement, $h = h_{LV}$ is the height, α_h = 2/3 defines the seismic force resultant position; assuming a triangular distribution (Doherty et al., 2002; Degli Abbati and Lagomarsino, 2017), E_m is the masonry Young's modulus, B is the width, t is the thickness, $W = h\ t\ B\ \gamma_m$ is the weight, N is the vertical force at the top of the wall and f_{mb} is the compressive strength of the masonry units. In Figure 1 the comparison between analytical results and two experimental tests from (Degli Abbati and Lagomarsino, 2017) and (Griffith et al., 2004) are reported.

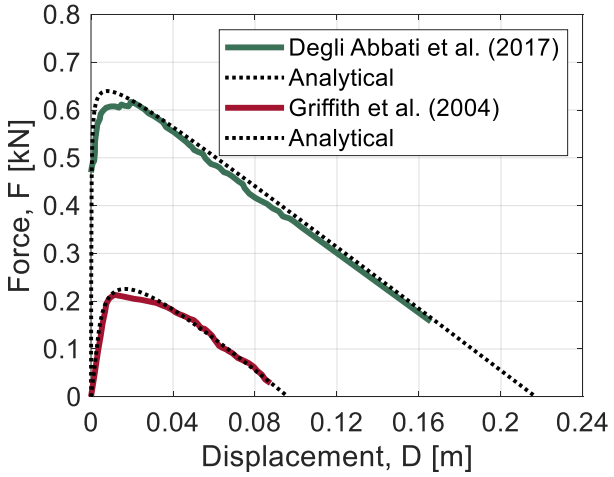

Figure 1. Comparison between experimental OOP F-D curves by (Griffith et al., 2004; Degli Abbati and Lagomarsino, 2017) and analytical solutions.

3 PARAMETERS UNCERTAINTY

From Equations 1 and 2, seven relevant input parameters affecting the OOP capacity are selected. Among the geometrical variables h and t are considered. Width B is assumed constant instead and equal to 1.0 m. Once the F-D curve is reported in a Spectral Acceleration (S_a) versus Spectral Displacement (S_d) plane (Doherty et al., 2002; Lagomarsino, 2015), it is not dependant on the width B.

Material parameters included in the sensitivity analysis are E_m, γ_m and f_{mb}. The last two parameters are related to the vertical overburden: q is the roof overload per unitary surface while s is the midspan of the roofing structure (simply supported assumption). In Figure 2 typical one-story brick in mud-mortar school buildings with light Corrugated Galvanized Iron (CGI) roof are shown. The statistical characterization of the constituting walls of this building typology are described in the following section.

Figure 2. Typical one-story brick school building (source: SAFER, 2019a).

3.1 PDF of input parameters

Input variables of the considered structural typology are described through specific probability distribution function (PDF) as in (Giordano et al., 2019). In details:

- h is modelled with a truncated normal PDF having mean $\mu(h)$ = 2.7 m, coefficient of variation $CoV(h)$ = 0.3, lower bound $min(h)$ = 2.4 m and upper limit $max(h)$ = 3.0 m (ARUP, 2015);
- t is represented by a uniform PDF with $min(t)$ = 0.35 m and $max(t)$ = 0.45 m (ARUP, 2015);
- E_m is described by a lognormal PDF with $\mu(E_m)$ = 537.25 MPa and $CoV(E_m)$ = 0.469 (Research Center for Disaster Mitigation of Urban Cultural Heritage, 2012);
- γ_m is represented by a lognormal PDF having $\mu(\gamma_m)$ = 17.68 MPa (Research Center for Disaster Mitigation of Urban Cultural Heritage, 2012) and $CoV(\gamma_m)$ = 0.05 (JCSS, 2001);
- q is assumed with a lognormal PDF having $\mu(q)$ = 0.15 kN/m^2 and $CoV(q)$ = 0.22 (Bureau of Indian Standards (BIS), 1987);
- s is described by a normal truncated PDF with $\mu(s)$ = 1.5 m, $CoV(s)$ = 0.3, $min(s)$ = 1 m and $max(s)$ = 2 m (National Society for Earthquake Technology, NSET, 2000).

The masonry unit compressive strength f_{mb} has been quantified through experimental tests carried out at the Tribhuvan University (SAFER, 2019b). The results of six 23 cm × 10 cm × 6.35 cm fired bricks are reported in Table 1. Figure 3 shows the test setup. The statistical results of the experimental campaign are $\mu(f_{mb})$ = 5.97 MPa and $CoV(f_{mb})$ = 0.29. A lognormal PDF is considered for this variable.

Table 1. Results of compressive tests on fired bricks.

Test N	Breaking load [kN]	f_{mb} [MPa]
1	180	7.83
2	185	8.04
3	112	4.87
4	133	5.78
5	79	3.43
6	135	5.87
μ	137.3	5.97
CoV	0.29	0.29

Figure 3. Experimental setup for compressive tests of fired bricks carried out at the Tribhuvan University (SAFER, 2019b).

It is worth mentioning that $\mu(f_{mb})$ results consistently lower that the value indicated by Phaiju and Pradhan (2018) i.e., 11.12 MPa. Large scatter of brick strength is indeed very common in Nepal since industrial production processes are not rigorously implemented and there is a significant difference in mechanical properties of bricks based on the area in Nepal.

4 TORNADO ANALYSIS

4.1 Methodology

Tornado diagrams are classic statistical tools for sensitivity analysis and decision making (Eschenbach, 2006) widely used in earthquake engineering applications (Porter et al., 2002).

In this study tornado diagrams are derived to quantify the variability of OOP *F-D* results with respect to the seven input parameters discussed in Section 3.1. As described by Celarec et al. (2012), the first step of the sensitivity analysis is to estimate the model output for the central values (50th percentiles) of the input parameters. Subsequently, the model is relaunched by varying the input parameters at their 16th and 84th percentile one at time (Table 2). Referring to the considered case, this leads to a total of 14 parameter combinations.

Four output parameters representative of the *F-D* curve are considered in the analysis:

- the maximum OOP force capacity of the wall F_{max};
- the corresponding displacement D_{peak};

- the maximum displacement capacity D_{max} that corresponds to the minimum between toe compressive failure at the base of the wall (brick crashing) or wall overturning (null force capacity);
- the secant negative stiffness of the post peak slope K_s calculated with the following formula:

$$K_s = \frac{F_{max} - F_{Dmax}}{D_{max} - D_{peak}} \quad (3)$$

where F_{Dmax} is the residual force at D_{max}.

Table 2. Input values for the sensitivity analysis.

Input	Percentile		
	16th	50th	84th
h [m]	2.50	2.70	2.90
t [m]	0.366	0.400	0.434
E_m [MPa]	312.2	486.4	757.8
γ_m [kN/m^3]	16.80	17.66	18.56
q [kN/m^2]	0.119	0.148	0.184
s [m]	1.20	1.50	1.80
f_{mb} [MPa]	4.30	5.72	7.63

In Figure 4 the described output parameters are schematically represented.

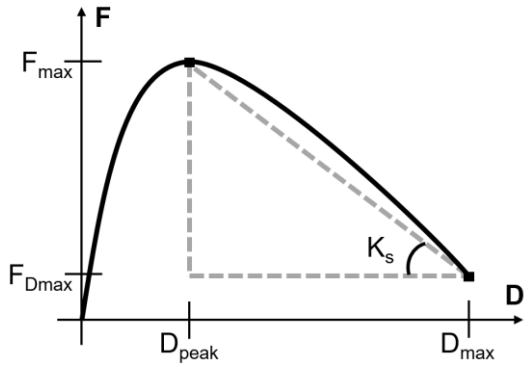

Figure 4. Output parameters considered for the sensitivity analysis.

The variability of the output quantities with respect to the input values is calculated as in (Celarec et al., 2012):

$$\Delta x = \frac{x_{i,j} - x_{cv}}{x_{cv}} \cdot 100 \quad (4)$$

where: Δx is the percentage variation of the output x with respect to his central value x_{cv}, $x_{i,j}$ is the output value obtained by varying the i^{th} input parameter to the j^{th} percentile (16th or 84th).

4.2 *Discussion of the results*

Figure 5 reports the *F-D* curves evaluated with the closed/form solution reported in Equations 1 and 2. In details, the diagram calculated with the central values is indicated by the solid black line while the 14 sensitivity combinations are represented by the grey lines. The resulting 15 curves have been processed to extract the four output parameters for the tornado diagrams.

In the following, the results of the sensitivity analysis are discussed.

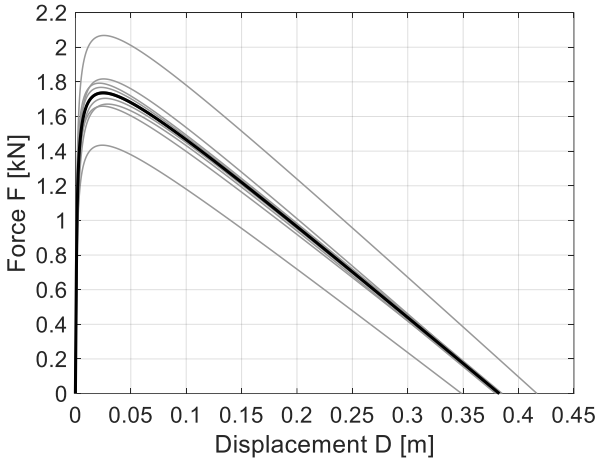

Figure 5. *F-D* curves of the representative URM wall: the black line is calculated with the central values of the input parameters while the grey lines correspond to the 14 combinations of the sensitivity analysis.

4.2.1 *Sensitivity of F_{max}*

Figure 6 reports the tornado diagram related to the maximum OOP force capacity of the wall. It can be observed that the variation of the thickness of the wall generates a variation of the output value of about ±18%.

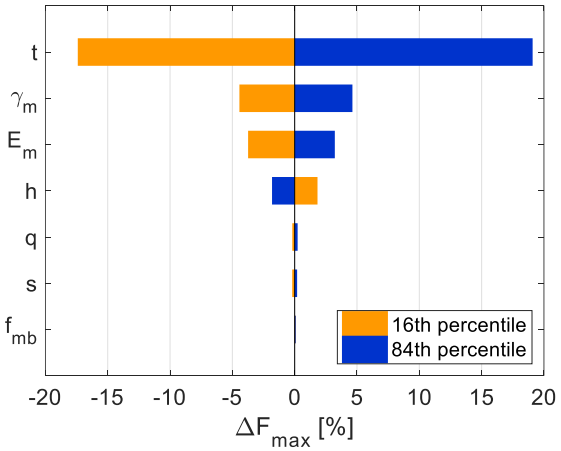

Figure 6. Tornado diagram for maximum force capacity (F_{max}).

The unit weight of the masonry material is the second most influential parameter and influence

the results of ±5%. Similarly, the variation of the elastic modulus affects the output approximately of ±4%. The remaining parameters have instead a negligible effect on the maximum force capacity. The effect of the variation of the wall height over the output is less than 3%. Additionally, given the light weight of CGI roofing systems, q and s provide percentage variations of F_{max} almost equal to zero.

4.2.2 *Sensitivity of D_{peak}*

In Figure 7 the tornado diagram related to the displacement at peak is reported. It can be observed that the elastic modulus has the largest influence on the output. The percentage variation is in the range of ±15%.

The second most important parameter is the height of the wall with a variation of about ±7%. The remaining parameters have a slight effect on the output.

The thickness displays a variation of about ±2.5%, consistently lower than the one estimated for F_{max}. Similarly, the quantities related to the static loads (i.e. γ_m, q, s) have no significant influence on D_{peak}.

4.2.3 *Sensitivity of D_{max}*

Figure 8 reports the sensitivity results for the maximum displacement. As expected, D_{max} is exclusively governed by the thickness of the wall which generates a ±9% variation of the output. The remaining parameters have an influence smaller than ±1%. Given the considered structural configuration (i.e., one-story cantilever wall supporting a light CGI roof), D_{max} corresponds to the overturning condition (null force). Therefore, the variation of the compressive strength of the units does not affect the output. This situation might not occur when analysing other wall configurations.

For example, it was observed that the failure mode switch to material crashing when the vertical loads on the URM wall are more severe (Giordano et al. 2017). It is worth mentioning that the results in Figure 7 and 8 are consistent with the physics of the problem; D_{peak} is mostly governed by the masonry mechanical properties, while D_{max} is solely defined by the geometrical nonlinearity (since no cases of toe crushing occurs in the case considered).

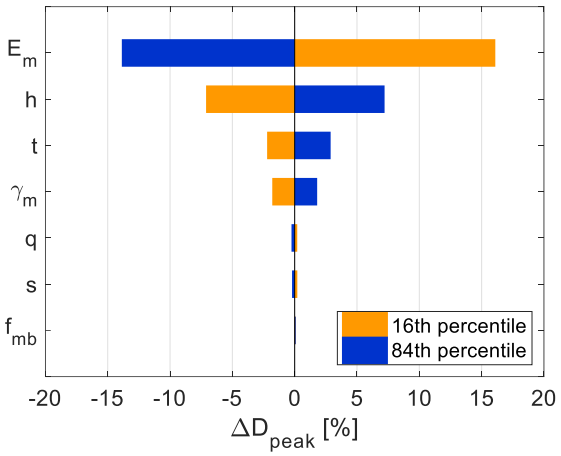

Figure 7. Tornado diagram for displacement at peak (D_{peak}).

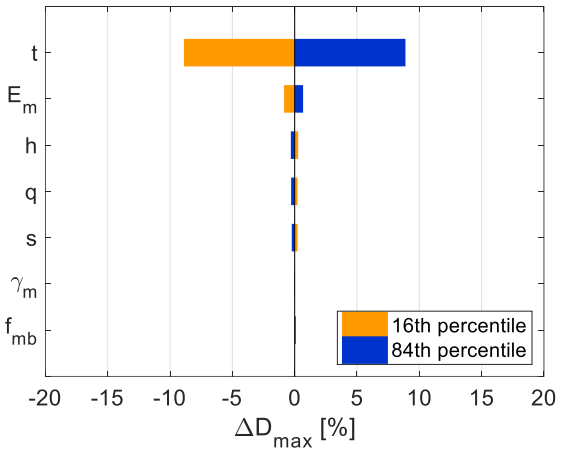

Figure 8. Tornado diagram for maximum displacement (D_{max}).

.

4.2.4 *Sensitivity of K_s*

The last sensitivity analysis is carried out on the quantity K_s (Figure 9).

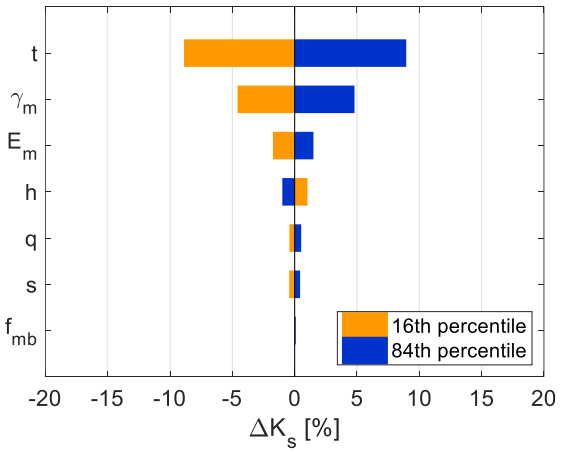

Figure 9. Tornado diagram for negative secant stiffness (K_s).

In this case the most influential parameter is the thickness of the wall. The effect over the output is

in the range of ±9%. The second relevant parameter is the masonry specific weight (±5%) while the remaining quantities affect the output for less than 2%.

5 CONCLUSIONS

In this work the sensitivity of OOP failure to input parameters of a URM Nepali wall has been investigated through the assessment of its F-D curve. A closed-form analytical model has been adopted to derive *F-D* curve. The results of the sensitivity analyses have been reported in the form of tornado diagrams. The study points out that wall thickness and masonry elastic modulus are the most influential parameters of the OOP capacity assessment. These quantities are followed by wall height and material density. Contrarywise, masonry compressive strength and roof characteristics (weight and span) are almost irrelevant in the analysis. These results should be considered valid only for the investigated building typology i.e., one-story brick-in-mud with light CGI roof. In particular, the CGI roof typology has an irrelevant weight with respect to the wall's weight and it does not provide any restraint.

In the view of executing vulnerability assessments at regional scale, the outcome of this sensitivity analysis can be used to prioritize data collection and experimental tests for this building typology. For instance, thickness is a parameter that can be collected through rapid surveys. Elastic modulus can be quantified on-site through flat-jack tests (e.g., Research Center for Disaster Mitigation of Urban Cultural Heritage, 2012) or in the laboratory by executing compressive tests on masonry wallets (e.g., Phaiju and Pradhan 2018). Both these techniques have been already adopted in the context of Nepal but further results are needed to better characterise the variability in different regions of the country (i.e., rural versus urban contexts). Lastly, γ_m requires further investigations since bricks density can change significantly from the Kathmandu Valley to the rest of country and the investigation available are not sufficient for a reliable characterisation.

ACKNOWLEDGEMENTS

This work was funded by the Engineering and Physical Science Research Council (EPSRC) under the project "Seismic Safety and Resilience of Schools in Nepal" SAFER (EP/P028926/1). http://www.safernepal.net/

REFERENCES

Ahmad, N., Ali, Q., Crowley, H., Pinho, R., 2014. Earthquake loss estimation of residential buildings in Pakistan, *Natural Hazards*, **73**(3), 1889–1955.

ARUP, 2015. *Global Program for Safer Schools - Structural Typologies*, London, UK.

Brando, G. et al., 2017. Damage Reconnaissance of Unreinforced Masonry Bearing Wall Buildings After the 2015 Gorkha, Nepal, Earthquake, *Earthquake Spectra*, **33**(S1), S243–S273.

Bureau of Indian Standards BIS, 1987. *IS 875: Code of Practice for Design Loads (Other Than Earthquake) For Buildings and Structures*, New Delhi, India.

Celarec, D., Ricci, P., Dolšek, M., 2012. The sensitivity of seismic response parameters to the uncertain modelling variables of masonry-infilled reinforced concrete frames, *Engineering Structures*, **35**, 165–177.

Ceran, H. B., Erberik, M. A., 2013. Effect of out-of-plane behavior on seismic fragility of masonry buildings in Turkey, *Bulletin of Earthquake Engineering*, **11**(5), 1775–1795.

D'Ayala, D. F., Paganoni, S., 2011. Assessment and analysis of damage in L'Aquila historic city centre after 6th April 2009, *Bulletin of Earthquake Engineering*, **9**(1), 81–104.

De Felice, G., Giannini, R., 2001. Out-of-plane seismic resistance of masonry walls, *Journal of Earthquake Engineering*, **5**(2), 253–271.

Degli Abbati, S., Lagomarsino, S., 2017. Out-of-plane static and dynamic response of masonry panels, *Engineering Structures*, **150**, 803–820.

De Luca, F., Giordano, N., Gryc, H., Hulme, L., McCarthy, C., Sanderson, V., Sextos, A., 2019. Nepalese School Building Stock and Implications on Seismic Vulnerability Assessment. *2nd International Conference on Earthquake Engineering and Post Disaster Reconstruction Planning*, Bhaktapur, Nepal.

Doherty, K., Griffith, M. C., Lam, N., & Wilson, J., 2002. Displacement-based seismic analysis for out-of-plane bending of unreinforced masonry walls, *Earthquake Engineering and Structural Dynamics*, **31**(4), 833–850.

Eschenbach, T. G., 2006. Technical Note: Constructing Tornado Diagrams with Spreadsheets, *The Engineering Economist*, **51**(2), 195–204.

Ferreira, T. M., Costa, A. A., Costa, A., 2015a. Analysis of the out-of-plane seismic behavior of unreinforced masonry: A literature review, *International Journal of Architectural Heritage*, **9**(8), 949–972.

Ferreira, T. M., Costa, A. A., Vicente, R., Varum, H., 2015b. A simplified four-branch model for the analytical study of the out-of-plane performance of regular stone URM walls. *Engineering Structures*, **83**, 140–153.

Giaretton, M., Valluzzi, M. R., Mazzon, N., Modena, C., 2017. Out-of-plane shake-table tests of strengthened multi-

leaf stone masonry walls. *Bulletin of Earthquake Engineering*, **15**(10), 4299–4317.

Giordano, N., Crespi, P., Franchi, A., 2017. Flexural strength-ductility assessment of unreinforced masonry cross-sections: analytical expressions, *Engineering Structures*, **148**, 399–409.

Giordano, N., De Luca, F., Sextos, A., Maskey, P. N., 2019. Derivation of fragility curves for URM school buildings in Nepal, *ICASP13*, Seoul, South Korea.

Godio, M., Beyer, K., 2017. Analytical model for the out-of-plane response of vertically spanning unreinforced masonry walls, *Earthquake Engineering and Structural Dynamics*, **46**(15), 2757–2776.

Griffith, M. C., Lam, N. T. K., Wilson, J. L., Doherty, K., 2004. Experimental Investigation of Unreinforced Brick Masonry Walls in Flexure. *Journal of Structural Engineering*, **130**(3), 423–432.

JCSS, 2001. *Probabilistic Model Code - Part 2: Load Models*.

La Mendola, L., Papia, M., Zingone, G., 1995. Stability of Masonry Walls Subjected to Seismic Transverse Forces, *Journal of Structural Engineering*, **121**(11), 1581–1587.

Lagomarsino, S., 2015. Seismic assessment of rocking masonry structures, *Bulletin of Earthquake Engineering*, **13**(1), 97–128.

Lagomarsino, S., Cattari, S., 2015. PERPETUATE guidelines for seismic performance-based assessment of cultural heritage masonry structures, *Bulletin of Earthquake Engineering*, **13**(1), 13–47.

National Society for Earthquake Technology, 2000. *Seismic vulnerability of the public school buildings of Kathmandu Valley and methods for reducing it*, Kathmandu, Nepal.

Phaiju, S., Pradhan, P. M., 2018. Experimental Work for Mechanical Properties of Brick and Masonry Panel, *Journal of Science and Engineering Nepal*, **5**(8), 51–57.

Porter, K. A., Beck, J. L., Shaikhutdinov, R. V., 2002. Sensitivity of Building Loss Estimates to Major Uncertain Variables, *Earthquake Spectra*, **18**(4), 719–743.

Research Center for Disaster Mitigation of Urban Cultural Heritage, 2012. *Disaster Risk Management for the Historic City of Patan, Nepal*, Kyoto, Japan.

SAFER, 2019a. *Compressive Strength of Bricks (internal document)*, Tribhuvan University, Nepal.

SAFER, 2019b. *SAFER App database (internal webapp)*, University of Bristol, UK.

Sharma, K., Deng, L. and Noguez, C. C., 2016. Field investigation on the performance of building structures during the April 25, 2015, Gorkha earthquake in Nepal, *Engineering Structures*, **121**, 61–74.

Shawa, O. Al et al., 2012 Out-of-plane seismic behaviour of rocking masonry walls, *Earthquake Engineering and Structural Dynamics*, **41**(5), 949–968.